

NISTIR 5945

**Performance of R-22 Alternative Refrigerants in a
System with Cross-flow and Counter-flow
Heat Exchangers**

Man-Hoe Kim
Piotr A. Domanski
David A. Didion

Building and Fire Research Laboratory
Gaithersburg, Maryland 20899



United States Department of Commerce
Technology Administration
National Institute of Standards and Technology

Performance of R-22 Alternative Refrigerants in a System with Cross-flow and Counter-flow Heat Exchangers

Man-Hoe Kim
Piotr A. Domanski
David A. Didion

January 1997



U.S. Department of Commerce
Michael Kantor, *Secretary*
Technology Administration
Mary L. Good, *Under Secretary for Technology*
National Institute of Standards and Technology
Arati Prabhakar, *Director*

Prepared for:
U.S. Department of Energy
William Noel, Project Manager
Office of Building Technology
Building Equipment Division
1000 Independence Ave., SW
Washington, DC 20585

ABSTRACT

This report presents results of performance tests of R-22 and four alternative fluids, R-134a, R-32/134a (30/70), R-407C, and R-410A, at operating conditions typical for a residential heat pump. The study was performed in an experimental breadboard water-to-water heat pump in which a water/ethylene glycol mixture was used as the heat-transfer fluid. The heat exchangers representing the indoor and outdoor coils were counter-flow and cross-flow, respectively. The cooling tests were conducted for all five fluids, and the heating tests were run for R-22 and R-407C. The report presents test results for the system and data characterizing the performance of the heat exchangers and compressor. The zeotropic mixtures, R-32/134a and R-407A, had similar performance characteristics as R-22. At tests performed at the same capacity, R-410A had the highest Coefficient of Performance.

Key Words: air conditioning, heat pump, heat transfer, refrigerant, refrigeration, thermodynamics.

ACKNOWLEDGMENT

This study was conducted under the sponsorship of the U.S. Department of Energy, Office of Building Technology, Building Equipment Division with Mr. William Noel serving as Program Manager.

TABLE OF CONTENTS

ABSTRACT	iii
ACKNOWLEDGMENT	iv
TABLE OF CONTENTS	v
LIST OF TABLES	vi
LIST OF FIGURES	vii
NOMENCLATURE	ix
1. INTRODUCTION	1
2. EXPERIMENTAL APPARATUS	1
3. REFRIGERANTS SELECTED	2
4. EXPERIMENTAL PROCEDURE	3
5. TEST RESULTS	4
5.1 Cooling Test Results for the Basic System	4
5.2 Cooling Test Results for the System with LLSL-HX	6
5.3 Cooling and Heating Results for R-22 and R-407C	7
6. CONCLUDING REMARKS	8
7. REFERENCES	9
8. APPENDIX. Data Uncertainty Information	20

LIST OF TABLES

1. Refrigerants Considered in the Study	2
2. Heat Transfer Fluid Temperatures	3
3. Summary of Results for R-407C and R-22 from Tests at 1000 Compressor RPM	10
A1. Summary of Uncertainty Analysis	20

LIST OF FIGURES

1. Schematic of the Small Breadboard Heat Pump	11
2. Vapor Pressures for Refrigerants Studied	11
3. Capacity and COP of the Basic System During Test A for 1000 and 1800 Compressor RPM	12
4. Refrigerant Mass Flow Rate in the Basic System During the Cooling Test (1800 Compressor RPM)	12
5. Compressor Discharge Pressure for the Basic System During the Cooling Test (1800 Compressor RPM)	13
6. Compressor Discharge Temperature for the Basic System During the Cooling Test (1800 Compressor RPM)	13
7. Temperature Distribution of R-22 in Cross-Flow Condenser and Counter-Flow Evaporator During the Cooling Test (Basic System, 1800 Compressor RPM)	14
8. Temperature Distribution of R-407C in Cross-Flow Condenser and Counter-Flow Evaporator During the Cooling Test (Basic System, 1800 Compressor RPM)	14
9. Refrigerant Pressure Drop in Cross-Flow Condenser and Counter-Flow Evaporator During the Cooling Test (Basic System, 1800 Compressor RPM)	15
10. Dew Point dT/dP for Refrigerants Studied	15
11. UA Values for Evaporator and Condenser During the Cooling Test (Basic System, 1800 Compressor RPM)	16
12. Capacity During the Cooling Test (System with LLSL-HX, 1800 Compressor RPM)	16
13. Compressor Power During the Cooling Test (System with LLSL-HX, 1800 Compressor RPM)	17
14. COP During the Cooling Test (System with LLSL-HX, 1800 Compressor RPM)	17
15. Capacity of LLSL-HX During the Cooling Test (1800 Compressor RPM)	18

16.	Pressure-Enthalpy Diagram for R-22 During the Cooling Test at Different Superheat at the LLSL-HX Outlet (1800 Compressor RPM)	18
17.	Refrigerant Pressure Drop in the Cross-Flow Condenser During the Cooling Test (System with LLSL-HX, 1800 Compressor RPM)	19
18.	Refrigerant Pressure Drop in the Counter-Flow Evaporator During the Cooling Test (System with LLSL-HX, 1800 Compressor RPM)	19

NOMENCLATURE

COP	- coefficient of performance
c_p	- molar heat capacity
HTF	- heat-transfer fluid
h	- enthalpy
LLSL-HX	- liquid-line/suction-line heat exchanger
\dot{m}	- mass flow rate
\dot{Q}	- capacity
RMS	- root mean square
SBHP	- Small Breadboard Heat Pump
T	- temperature
UA	- overall heat-transfer conductance
u	- standard uncertainty
V	- volume
\dot{W}_{comp}	- compressor power

Subscripts

cond	- condenser
crit	- critical
evap	- evaporator
hx	- heat exchanger
sat	- saturation
vol	- volumetric

1. INTRODUCTION

The Montreal Protocol [1] established a schedule for elimination of chlorine-containing refrigerants, including R-22. This stimulated an intensive effort to find suitable replacement fluids for various applications. The goal of this study was to experimentally evaluate hydrofluorocarbon R-22 alternatives for use in a residential air-to-air heat pump. Five fluids were tested: R-22, R-134a, R-32/134a, R-407C, and R-410A.

2. EXPERIMENTAL APPARATUS

The experimental apparatus, referred to as a Small Breadboard Heat Pump (SBHP), was composed of the basic elements of the refrigeration system (compressor, evaporator, condenser, expansion device, and liquid-line/suction-line heat exchanger), the heat-transfer-fluid (HTF) circulation system (pumps, fluid containers), and the data acquisition system. A water/ethylene glycol mixture (60/40 by mass) was used as the heat-transfer fluid in both heat exchangers. The SBHP was used in several projects undertaken at the National Institute of Standards and Technology (NIST), starting with the investigation by Pannock and Didion [2]. For this study, a cross-flow heat exchanger was incorporated to the system. Figure 1 shows a schematic of the SBHP.

The SBHP used an open-type, two-cylinder, reciprocating compressor of 45 cm³ displacement. The mineral oil that was originally supplied with the compressor was used with all five refrigerants tested. An inverter was installed to alter the compressor speed within the 500-3000 RPM range. A dynamometer attached to the shaft between the motor and compressor allowed for measurement of speed and torque. The outdoor coil was represented by a cross-flow heat exchanger made of eighteen identical segments. They were connected in series for the refrigerant, but in parallel for the HTF. The segments consisted of two concentric, circular tubes. The refrigerant was flowing through the inner tube, and the heat-transfer fluid was flowing through the annular space filled with spiny fins. Each segment had six inlets and five outlets for the HTF. They were evenly spaced over the segment's length to ensure cross flow of the HTF relative to the refrigerant flow. This cross-flow arrangement corresponded to a typical heat-transfer configuration of the residential system's outdoor coil, which usually is only one or two tubes deep.

The indoor coil was represented by a counter-flow heat exchanger composed of twenty segments. These segments were similar to the condenser's segments with the exception that the HTF's inlet and outlet were at the opposing ends of each segment. The segments were connected in series to obtain a counter-flow arrangement. This arrangement corresponds to the optimum design limit of the indoor coil in which some degree of cross-counter flow configuration is attainable with three to five tube-depth rows.

The SBHP included a conventional liquid-line/suction-line heat exchanger (LLSL-HX). The SBHP was also equipped with a refrigerant-charging unit, which could regulate the amount and composition (for zeotropes) of refrigerant in the system. For a zeotropic mixture, if liquid refrigerant was leaving the condenser and was stored in the charging unit, and the vapor refrigerant was let into the

evaporator from this unit, the amount of more volatile component in the circulating mixture increased.

Refrigerant temperature and pressure were measured by thermocouples and pressure transducers placed in the key locations of the refrigerant loop. Additionally, thermocouples were attached throughout the heat exchangers to measure the temperature profiles of the refrigerant and HTF. Temperature change of the HTF was measured by thermopiles located at the inlet and outlet of the condenser and evaporator. A data acquisition/control unit connected to a personal computer enabled the system operation, test condition control, and test data collection. The data uncertainty information is presented in the Appendix.

3. REFRIGERANTS SELECTED

Refrigerant 22 and four alternative working fluids were studied. Table 1 contains their basic thermodynamic parameters, and Figure 2 shows their vapor pressure curves. From Table 1, the near-azeotrope R-32/125 (50/50) is the most volatile fluid, and R-134a has the lowest volatility. The zeotropes R-32/125/134a (23/25/52) and R-32/134a have similar thermodynamic characteristics, but the latter is marginally flammable. All refrigerant properties during data collection and analysis were calculated using the REFPROP [3] implementation of the Carnahan-Starling-DeSantis equation of state. The mixtures R-32/125 (50/50) and R-32/125/134a (23/25/52) have ASHRAE designations R-410A and R-407C, respectively [4]. These designations are further used in this report.

Table 1. Refrigerants Considered in the Study

	Refrigerant	Mass fraction	$T_{\text{bubble point}}^{(1)}$	$T_{\text{glide}}^{(2)}$	T_{crit}	Molar mass	$c_p^{(3)}$
		%	°C	°C	°C	kg/kmol	kJ/kmol
1	R-22	100	-40.8	0	96.2	86.47	50.37
2	R-134a	100	-26.0	0	101.2	102.03	76.93
3	R-32/134a	30/70	-41.9	7.4	103.1 ⁽⁴⁾	79.19	59.03
4	R-32/125/134a ⁽⁵⁾	23/25/52	-43.8	7.1	97.5 ⁽⁴⁾	95.03	69.51
5	R-32/125 ⁽⁶⁾	50/50	-51.4	0.1	84.9 ⁽⁴⁾	86.03	61.10

⁽¹⁾ at atmospheric pressure (101.325 kPa)

⁽²⁾ $T_{\text{glide}} = T_{\text{dew point}} - T_{\text{bubble point}}$ at atmospheric pressure

⁽³⁾ saturated vapor at atmospheric pressure

⁽⁴⁾ REFPROP [3] estimates

⁽⁵⁾ R-407C

⁽⁶⁾ R-410A

4. EXPERIMENTAL PROCEDURE

After the system was evacuated, the refrigerant was charged in the liquid state through the valve located on the compressor suction side (see Figure 1). The top and bottom valves of the refrigerant charging unit were open at this time. Then, the system was turned on. The compressor speed was fixed to a desired value by controlling the inverter frequency, and the inlet and outlet HTF temperatures of the evaporator and condenser were maintained constant. When the heat pump system stabilized, all the valves of the refrigerant charging unit were closed.

Tests were performed for the basic vapor-compression system (comprising a compressor, condenser, expansion valve, and evaporator) and for the configuration that included the LLSL-HX. For all the tests, refrigerant subcooling at the condenser outlet was kept at $2^{\circ}\text{C} \pm 0.5^{\circ}\text{C}$. Refrigerant superheat at the basic system tests (without the LLSL-HX) was kept at $12^{\circ}\text{C} \pm 3^{\circ}\text{C}$, and it was between 2°C and 30°C during the tests with the LLSL-HX. Superheat and subcooling were controlled by adjusting the refrigerant charge and the opening of the expansion valve. For each test, the mass fraction of the circulating mixture was determined using a gas chromatograph. Refrigerant samples were taken through a valve located at the compressor discharge port. The SBHP charging unit was used to tune the circulating mixture to the desired mass fraction.

All fluids were tested for the cooling mode operation, and R-22 and R-407C were also tested in the heating mode. Table 2 shows the test conditions used in this study which correspond to the high-temperature cooling and heating tests for a residential heat pump [5]. The cooling tests were performed at the prescribed temperatures of the HTF entering and leaving the evaporator and condenser. The HTF temperature at the inlet to the evaporator was controlled by adjusting the thermal load of the variable heater. For the condenser, the inlet HTF temperature was set by adjusting the coolant (chilled water) flow in the HTF circulation system. The desired value of the outlet HTF temperatures in the evaporator and condenser were obtained by using a bypass to regulate the mass flow rate of the HTF passing through the heat exchangers. Only inlet HTF temperatures were specified for the heating mode tests. Instead of specifying the outlet temperatures, the mass

Table 2. Heat-transfer Fluid Temperatures

	cooling ($^{\circ}\text{C}$)	heating ($^{\circ}\text{C}$)
condenser inlet	35.0	21.1
condenser outlet	43.2	$m_{\text{evaporator,cooling}}$
evaporator inlet	26.7	8.3
evaporator outlet	14.4	$m_{\text{condenser,cooling}}$

$m_{\text{evaporator,cooling}}$ - HTF mass flow rate through the condenser during cooling test

$m_{\text{condenser,cooling}}$ - HTF mass flow rate through the evaporator during cooling test

selected flow rates of HTF from the cooling test were imposed to ensure the operating compatibility of the SBHP with field-installed systems.

5. TEST RESULTS

5.1 Cooling Test Results for the Basic System

Figure 3 presents the capacity and the coefficient of performance (COP) at two compressor speeds, 1000 RPM and 1800 RPM. At 1800 RPM, the capacities of R-22, R-407C, and R-32/134a are very similar, while the capacity of R-410A is 40% greater than the R-22 baseline, and the capacity of R-134a is 32% below the baseline. Among the three fluids having a similar capacity, R-22 and R-407C have an almost identical COP, and the COP of R-32/134a COP is 4.7% greater than that of R-22. The low-capacity R-134a shows only 2% COP improvement over R-22, while R-410A COP was 7% below the R-22 baseline.

The capacity of R-410A at 1000 RPM (3644 W) is almost the same as the capacity of R-22 at 1800 RPM (3663 W); however, the COP of R-410A is higher by 22%. Lower friction losses of the compressor at the lower compressor speed probably contributed to a higher COP of R-410A. We can make a similar comparison between R-22 and R-407C at 1000 RPM and R-134a COP at 1800 RPM; these fluids have a similar capacity but the COP of R-134a is much lower than that of R-22 and R-407C. The negative effect of the higher RPM on the compressor efficiency (through higher friction losses) and on the pressure drop in heat exchangers (through a higher volumetric flow) may explain the low COP of R-134a.

Figures 4, 5, and 6 show the refrigerant mass flow rate, compressor discharge pressure, and compressor discharge temperature at 1800 RPM. The refrigerant mass flow rate was determined from the refrigerant enthalpy change in the condenser and HTF's heat capacity and mass flow rate. The refrigerant states at the inlet and outlet of the condenser and compressor were determined from the temperature and pressure measurements at these locations. The mass flow rates of R-407C, R-410A, and R-32/134a are within 10% of the mass flow rate for R-22, and the mass flow rate of R-134a is much lower. The highest discharge pressure was measured for R-410A (3.2 MPa), which was significantly above the R-22 baseline (2.0 MPa). The two zeotropic mixtures had a discharge pressure similar to that of R-22, and the R-134a pressure was lower. Despite the high discharge pressure, the discharge temperature of R-410A was just a few degrees higher than that for R-22. The discharge temperatures for the remaining working fluids were below the R-22 baseline. This was due to the high heat capacity of R-134a.

Temperature profiles for the refrigerant and HTF provide an interesting insight into the operation of the counter-flow evaporator and cross-flow condenser, as given in Figures 7 and 8 for R-22 and R-407C, respectively. The temperature distribution in a cross-flow condenser was expected to be different from that of the counter-flow type. At any location, the entering temperature of the HTF is the same, while the exit temperature profile has a slope. For R-22 (Figure 7), this is mainly caused by a changing refrigerant heat-transfer coefficient, which (generally) is greater at higher than at lower

refrigerant qualities. For the zeotropic mixture (Figure 8), the slope of the HTF temperature line is more pronounced because of the glide of the mixture's saturation temperature during a phase change. The temperature profile of R-407C is horizontal in most of the evaporator, which indicates that the saturation temperature drop due to pressure drop offsets the mixture's temperature glide due to phase change.

Figure 9 presents pressure drops in the evaporator and condenser. The pressure drop in the evaporator is much greater than in the condenser because of higher specific volume and flow velocity. The most volatile (highest-pressure and most dense vapor) fluid, R-410A, had the highest pressure drop, and the low-volatile R-134a had the lowest. We should note that at the same absolute pressure a change in saturation temperature with a change in pressure, dT/dP , is greater for low pressure refrigerants. This may be seen in Figure 10, where it may also be noted that temperature changes with pressure increases significantly at lower temperatures. Thus, a given pressure drop affects the performance of the heat exchangers to a smaller degree when a high pressure refrigerant is employed and, for a given refrigerant, in the evaporator more than in the condenser.

The overall heat-transfer conductances for the evaporator and condenser, UA_{hx} , are presented in Figure 11. The UA_{hx} value was calculated by the following equation:

$$UA_{hx} = \frac{Q_{hx}}{\Delta T_{hx}}$$

where: $\Delta T_{hx} = \sum (A_{sec}/A_{hx}) \Delta T_{sec}$

A_{sec} = area of individual section

A_{hx} = total heat exchanger area

ΔT_{sec} = log-mean temperature difference for an individual section of the heat exchanger calculated by one of the following three equations [6].

1) Cross-flow section with single-phase flow:

$$\Delta T_{sec} = \frac{T_{f,o} - T_{f,i}}{\ln \left(\frac{\frac{T_{r,i} - T_{r,o}}{T_{f,o} - T_{f,i}}}{\frac{T_{r,i} - T_{r,o}}{T_{f,o} - T_{f,i}} + \ln \left(\frac{T_{r,o} - T_{f,i}}{T_{r,i} - T_{f,i}} \right)} \right)}$$

2) Cross-flow section with two-phase flow:

$$\Delta T_{\text{sec}} = \frac{T_{f,i} - T_{f,o}}{\ln\left(\frac{T_{f,i} - T_r}{T_{f,o} - T_r}\right)}$$

3) Counter-flow section:

$$\Delta T_{\text{sec}} = \frac{(T_{f,i} - T_{r,o}) - (T_{f,o} - T_{r,i})}{\ln\left(\frac{T_{f,i} - T_{r,o}}{T_{f,o} - T_{r,i}}\right)}$$

In the above formulas, subscripts f , r , i , and o represent the heat-transfer fluid, refrigerant, and inlet and outlet of the heat exchanger section, respectively.

Before making a conclusion from Figure 11, we have to recognize that the UA_{hx} values were affected by different mass flow rates of the heat-transfer fluid. These different mass flow rates were imposed during the tests to assure the same HTF temperature for different capacity refrigerants. For this reason, R-410A and R-134a required the highest and the lowest HTF mass flow rate, respectively. Thus, we can only draw conclusions from the UA_{hx} information for the fluids of similar capacity, i.e., R-22, R-407C, and R-32/134a. Since both R-407C and R-32/134a had a slightly greater cooling capacity than R-22 (Figure 3), we can state that the evaporation heat-transfer conductance of R-32/134a was better and that of R-407C was at least as good as the heat-transfer coefficient for R-22. This can be confirmed somewhat, at least qualitatively, in that R-407C has less R-32, which is known to have exceptional heat-transfer characteristics (i.e., low viscosity and high conductivity) compared to other halocarbons.

5.2 Cooling Test Results for the System with LLSL-HX

The tests with the LLSL-HX were performed with a constant condenser subcooling ($2\text{ }^{\circ}\text{C} \pm 0.5\text{ }^{\circ}\text{C}$) and with the compressor running at 1800 RPM. The main test variable was the superheat of refrigerant leaving the LLSL-HX. This superheat was set between $2\text{ }^{\circ}\text{C}$ and $30\text{ }^{\circ}\text{C}$ without imposing any constraints on the refrigerant state at the evaporator outlet. As a result, two-phase refrigerant entered the LLSL-HX during most of the tests.

It is important to note the significance of varying the superheat at the LLSL-HX outlet. Because the temperature difference between the high-pressure subcooled liquid and the low-pressure refrigerant varied with superheat, the LLSL-HX transferred a different amount of heat at different tests. The observed changes in the system performance are a result of heat transfer in the LLSL-HX and its

effect on the range of refrigerant quality in the evaporator. The latter phenomenon indirectly influences the system performance because the refrigerant's heat-transfer coefficient in the evaporator is quality dependent and particularly dependent on whether the low pressure fluid is superheated or two-phase. The impact of these influences could not be separated in this study.

Figure 12 presents the system cooling capacity. The capacity increases with the degree of superheat until the superheat range of 15 °C to 25 °C, above which the capacity decreases. Most likely, the maximum capacity coincides with the onset of superheating in the refrigerant at the evaporator outlet. The zeotropic mixtures, R-32/134a and R-407C, have the highest capacity. The compressor power was relatively unaffected by the refrigerant superheat, as shown in Figure 13. The relatively unchanged compressor power is a result of two opposing factors related to an increasing vapor superheat (specific volume): a higher compression work per unit mass of refrigerant and a lower refrigerant mass flow rate.

The COP increased for all fluids with the superheat increasing up to 15 °C to 20 °C (Figure 14). Compared to the COP obtained for the basic system (Figure 3), each fluid benefited from the installation of the LLSL-HX. This is also the case for R-22, whose COP with LLSL-HX shows little improvement in theoretical cycle calculations at fixed temperatures in the evaporator and condenser [7]. We may conclude that the system effects helped to improve COP_{R-22} . It is interesting to notice that for the single-component refrigerants, R-22 and R-134a, the COP values at a low superheat are almost the same (respectively) as the values from the basic system tests; however, for the two zeotropes, there is about 3% COP improvement when the LLSL-HX is used. This 3% COP improvement is due to the system effects with zeotropic mixtures, which are discussed by Vakil [8].

Figure 15 presents the capacity of the LLSL-HX. The capacity is the highest at small superheat primary because of a large temperature difference between the heat exchanging streams. At these low superheat values, the liquid leaving the condenser is subcooled to the evaporator saturation temperature, as shown in Figure 16. At high superheat, the capacity of the LLSL-HX is low because increased vapor temperature results in a small ΔT driving the heat transfer.

With the experiment run at the same subcooling at the condenser outlet, refrigerant pressure drop in the condenser was not affected by superheat (Figure 17), i.e., a small change in the pressure drop corresponds to the change observed in the refrigerant mass flow rate. For the evaporator (Figure 18), the pressure drop increased with increasing superheat at the LLSL-HX outlet because the average quality of refrigerant in the evaporator was higher at larger superheat.

5.3 Cooling and Heating Results for R-22 and R-407C

Because R-407C is widely considered as a “drop-in” replacement for R-22, additional tests were performed in the heating mode for R-407C and R-22. This section summarizes both the cooling and heating mode test results. In the cooling mode, the system employed the cross-flow heat exchanger as the condenser and the counter-flow heat exchanger as the evaporator. In the heating mode, the functions of the heat exchangers were reversed, i.e., the cross-flow evaporator and counter-flow

condenser were used. The tests of the system with the LLSL-HX were performed with 15 °C superheat at the LLSL-HX outlet. Other operating parameters were maintained within the same limits as for the tests reported in the previous sections.

Table 3 contains a summary of results from tests at 1000 compressor RPM. The cooling capacity of R-407C was a few percent greater than the capacity of R-22, while the heating capacities were almost the same. However, the COP of R-407C was lower than COP_{R-22} by 4 to 6 percent in both the cooling and heating modes. The use of the LLSL-HX did not significantly change the relative performance of the mixture and R-22.

Overall, the performance of R-407C is very similar to the performance of R-22. Small differences between capacity and COP exist, but they are different for different compressor speeds. For example, the COPs of the two fluids at the 1800 RPM cooling tests were practically, while R-407C was less efficient by 4 percent at 1000 RPM. We may speculate that the use of mineral oil could degrade the performance of R-407C (and other alternatives) at the lower RPM because of the refrigerant/oil immiscibility and less effective oil removal from the heat exchangers.

6. CONCLUDING REMARKS

The zeotropic mixtures, R-407C and R-32/134a (30/70), have the most similar performance characteristics to R-22, with R-32/134a having a slightly better COP. The important operating parameters (evaporator and condenser pressures and compressor discharge temperature) did not deviate significantly from the R-22 values. Also, the low-pressure R-134a had COP comparable to COP_{R-22} , but had a much lower capacity. The binary near-azeotrope, R-410A, displayed a 44% higher capacity than R-22 when tested at the same compressor RPM. At a reduced compressor speed at which R-410A capacity matched that of R-22, the COP of R-410A was 22% better than the COP of R-22. However, it has to be realized that this COP improvement resulted from significantly lower pressure losses (especially in the evaporator, suction line, and at compressor valves), and from reduced friction losses in the compressor running a lower speed.

Application of the LLSL-HX was beneficial to COPs of all fluids tested (R-410A was not included in these tests). For R-22 and R-134a, the COP was not improved when the heat was transferred to the two-phase refrigerant on the suction side (indicated by a low value of superheat leaving the LLSL-HX). For the zeotropic mixtures, R-407C and R-32/134a, a COP improvement was measured even at small values of superheat leaving the LLSL-HX. The benefits of this heat exchange between subcooled high-pressure liquid and two-phase low-pressure refrigerant has been hypothesized in literature, but has not been quantified and warrants further investigation.

It is difficult to objectively evaluate the performance potential of different fluids, even if the tests are performed in the same laboratory apparatus. The use of the same oil may penalize the refrigerants that are not miscible with it. If the same compressor speed is used for refrigerants of different capacities, different refrigerant saturation temperatures in the condenser and evaporator (needed to facilitate refrigerant-HTF heat transfer) penalize the higher capacity refrigerant with greater

compressor work. On the other hand, reducing compressor speed to obtain the same capacity also has a flaw because it reduces friction losses associated with the piston travel in the cylinder. It seems that the most practical approach is to calibrate the compressor for the RPM-related friction losses and to adjust the compressor work measured during a test. Also, using a compressor of the same design but smaller in capacity (i.e., bore or stroke) is another possibility. In either case, the impact of different refrigerant flow rates on pressure drop and heat-transfer coefficient should be considered.

7. REFERENCES

1. United Nations Environment Programme, Handbook for the Montreal Protocol on Substances that Deplete the Ozone Layer, Third Edition, Nairobi, Kenya, August, 1993.
2. J. Pannock and D.A. Didion, "The Performance of Chlorine Free Binary Zeotropic of Refrigerant Mixtures in a Heat Pump," NISTIR 4748, National Institute of Standards and Technology, Gaithersburg, MD, 1993.
3. J. Gallagher, M. McLinden, G. Morrison, and M. Huber, "NIST Thermodynamic Properties of Refrigerants and Refrigerant Mixtures Database (REFPROP)," Version 4.0, National Institute of Standards and Technology, Gaithersburg, MD, 1993.
4. ANSI/ASHRAE Standard 34-1992, "Number Designation and Safety Classification of Refrigerants," ASHRAE, Atlanta, GA, 1992.
5. ANSI/ASHRAE Standard 116-1995, "Methods of Testing for Rating for Seasonal Efficiency of Unitary Air Conditioners and Heat Pumps," ASHRAE, Atlanta, GA, 1995.
6. J.L. Threlkeld, "Thermal Environmental Engineering," Prentice-Hall, Inc., New Jersey, 1970.
7. P.A. Domanski, D.A. Didion, and J.P. Doyle, "Evaluation of Suction-Line/Liquid-Line Heat Exchange in the Refrigeration Cycle," International Journal of Refrigeration, Vol. 17, No. 7, 1994.
8. H.B. Vakil, "Thermodynamics of Heat Exchange in Refrigeration Cycles with Non-Azeotropic Mixtures," Part II: Suction Line Heat Exchange and Evaporative Cooling of Capillary, Proceedings of the International Congress of Refrigeration, International Institute of Refrigeration, Paris, 1983.
9. B.N. Taylor and C.E. Kuyatt, "Guidelines for Evaluating and Expressing the Uncertainty of NIST Measurement Results," NIST Technical Note 1297, 1994 Edition, National Institute of Standards and Technology, Gaithersburg, MD, 1994.
10. J. Gebbie, Rensselaer Polytechnic Institute, Troy, NY, private communication, 1996.

Table 3. Summary of Results for R-407C and R-22 from Tests at 1000 Compressor RPM
(see Appendix for uncertainty analysis)

Test	R-32/125/134a mass fraction %	R-407C value / R-22 value (ratio of R-407C value to R-22 value)				Compressor discharge (R-407C value - R-22 value)	
		capacity W	COP	\dot{Q}_{vol} kJ/m ³	refrigerant mass flow rate g/sec	pressure kPa	temperature °C
cooling	23.5/26.9/49.6	2630/2570 (1.02)	4.07/4.26 (0.96)	4443/4429 (1.00)	15.6/15.4 (1.01)	1962-1881=81	78-85=-7
cooling _{LLSL-HX}	23.2/26.7/50.1	2761/2673 (1.03)	4.28/4.46 (0.96)	4604/4506 (1.02)	15.5/15.1 (1.03)	1951-1891=60	86-94=-8
heating	22.3/26.1/51.6	2209/2213 (1.00)	4.42/4.72 (0.94)	3384/3427 (0.99)	10.6/10.7 (0.99)	1496-1397=99	64-72=-8
heating _{LLSL-HX}	21.8/25.6/52.6	2248/2231 (1.01)	4.61/4.86 (0.95)	3459/3443 (1.00)	10.4/10.5 (0.99)	1484-1385=99	74-82=-8

cooling - cooling test, basic system
cooling_{LLSL-HX} - cooling test, system with LLSL-HX
heating - heating test, basic system
heating_{LLSL-HX} - heating test, system with LLSL-HX

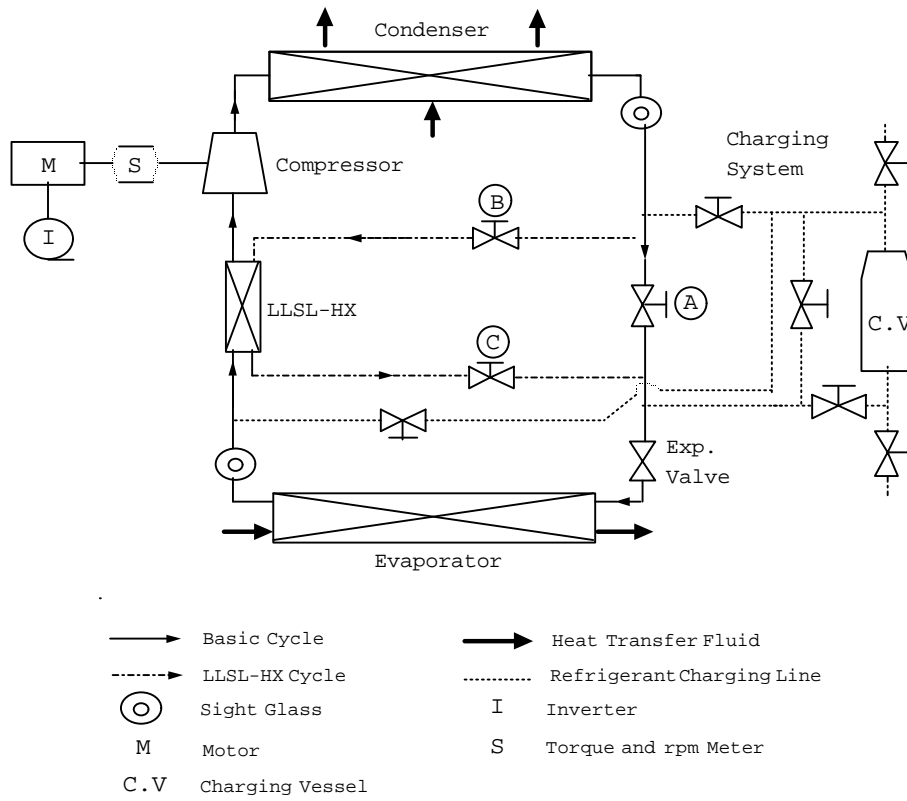


Figure 1 Schematic of the Small Breadboard Heat Pump

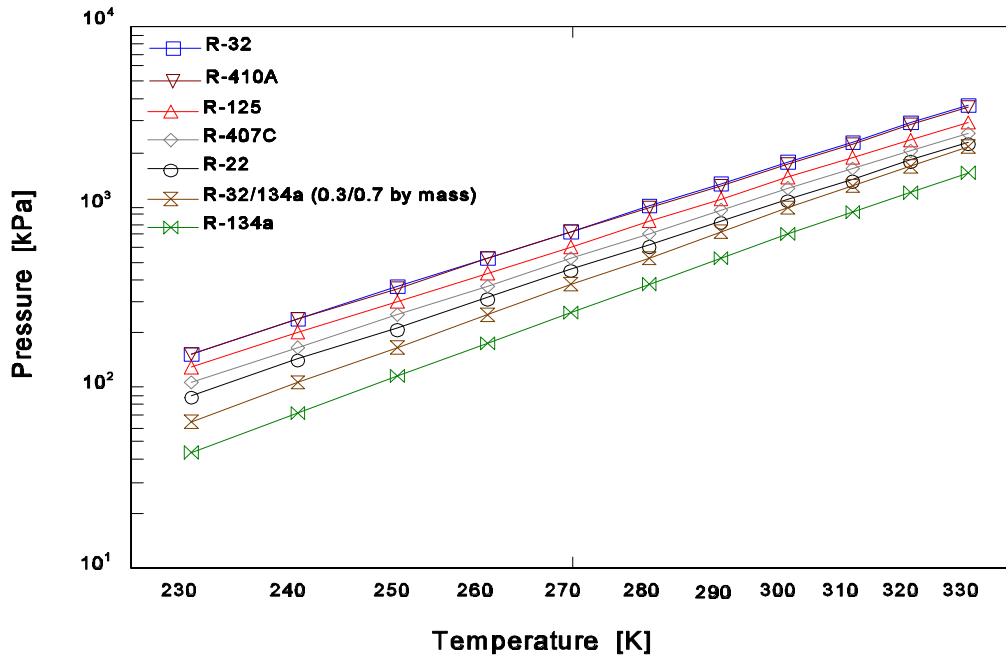


Figure 2. Dew Point Vapor Pressures for Refrigerants Studied

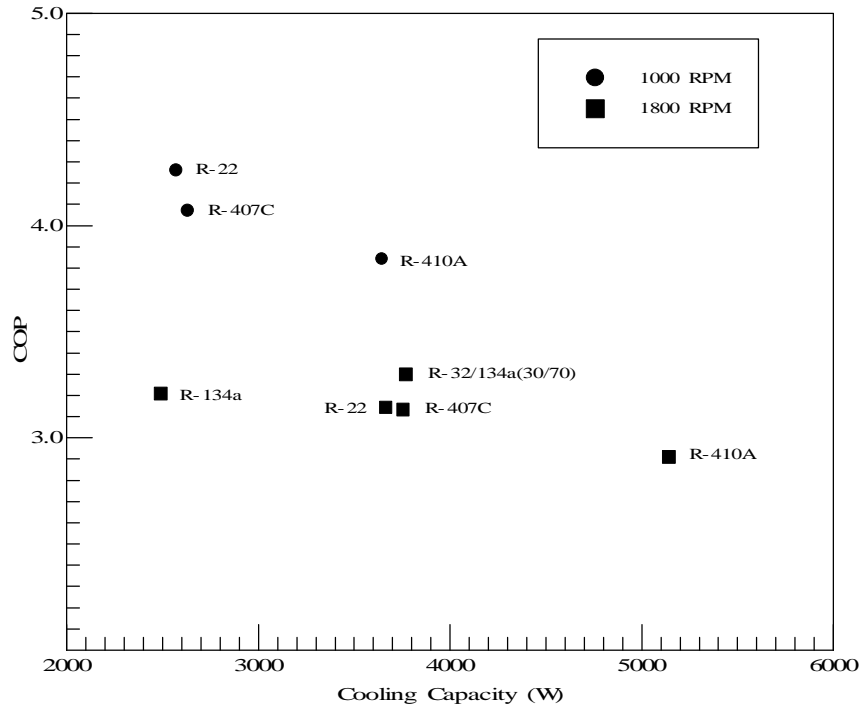


Figure 3. Capacity and COP of the Basic System During Test A for 1000 and 1800 Compressor RPM

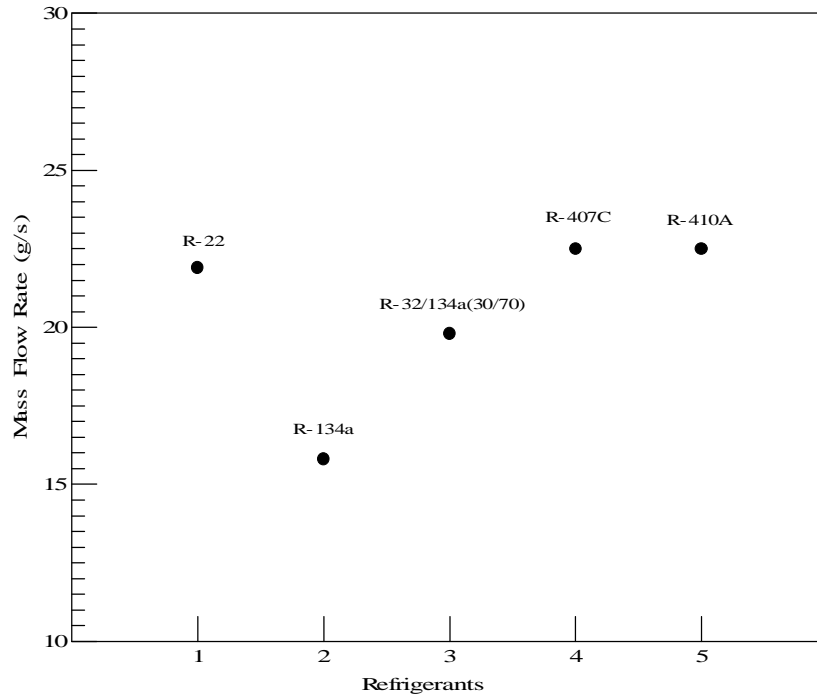


Figure 4. Refrigerant Mass Flow Rate in the Basic System During the Cooling Test (1800 Compressor RPM)

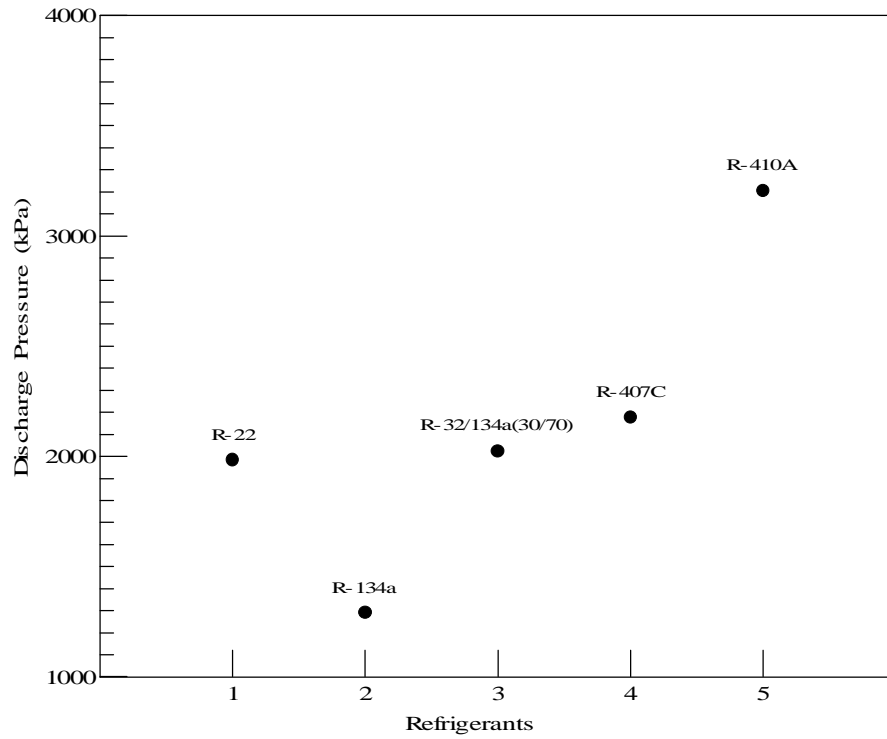


Figure 5. Compressor Discharge Pressure for the Basic System During the Cooling Test (1800 Compressor RPM)

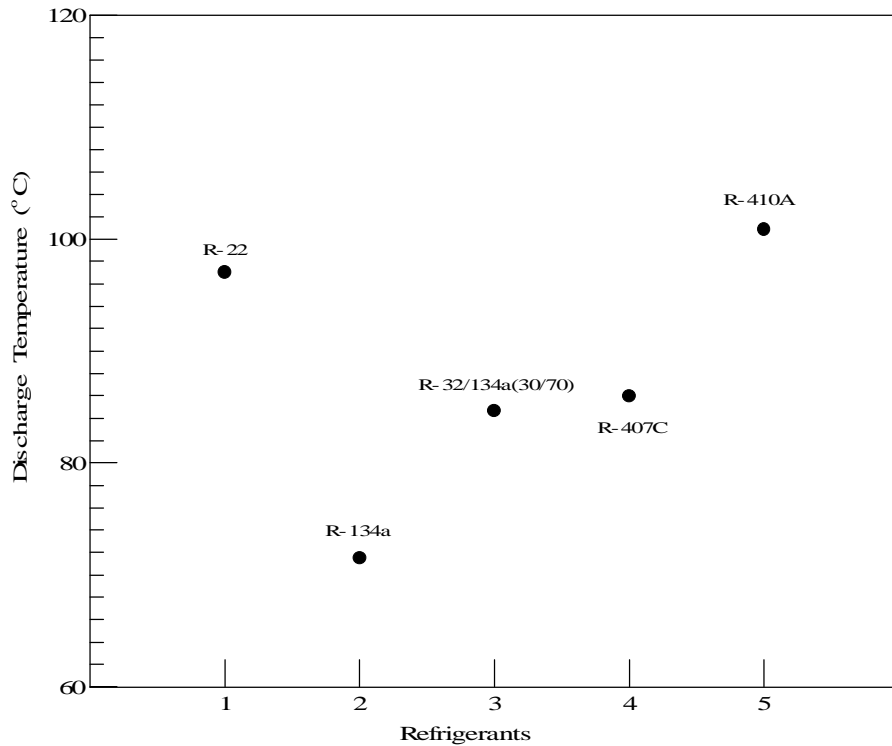


Figure 6. Compressor Discharge Temperature for the Basic System During the Cooling Test (1800 Compressor RPM)

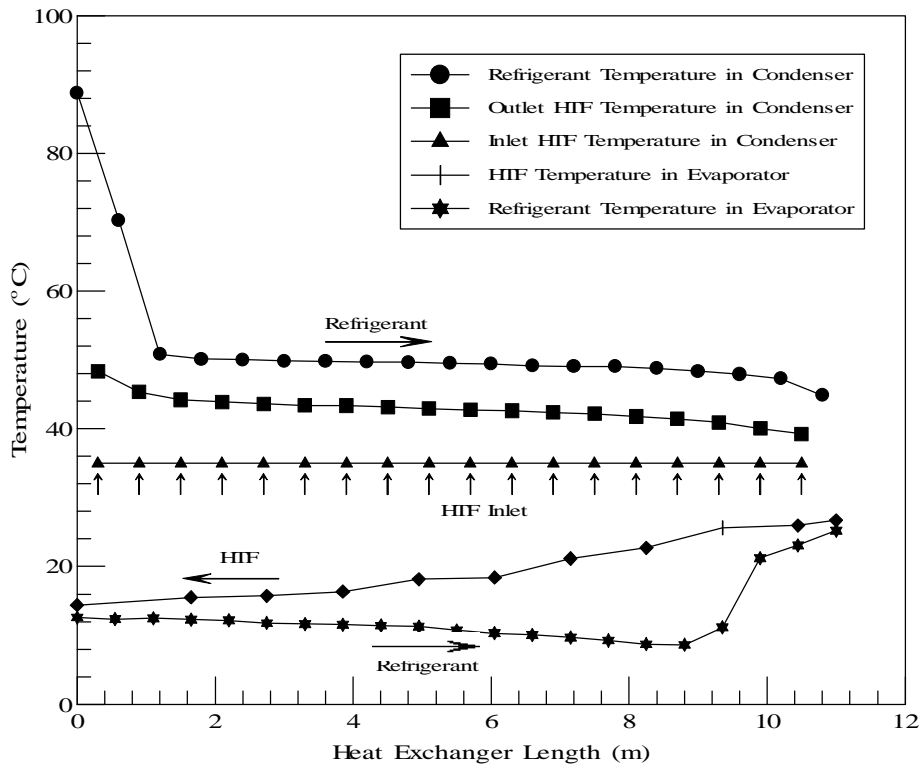


Figure 7. Temperature Distribution of R-22 in Cross-Flow Condenser and Counter-Flow Evaporator During the Cooling Test (Basic System, 1800 Compressor RPM)

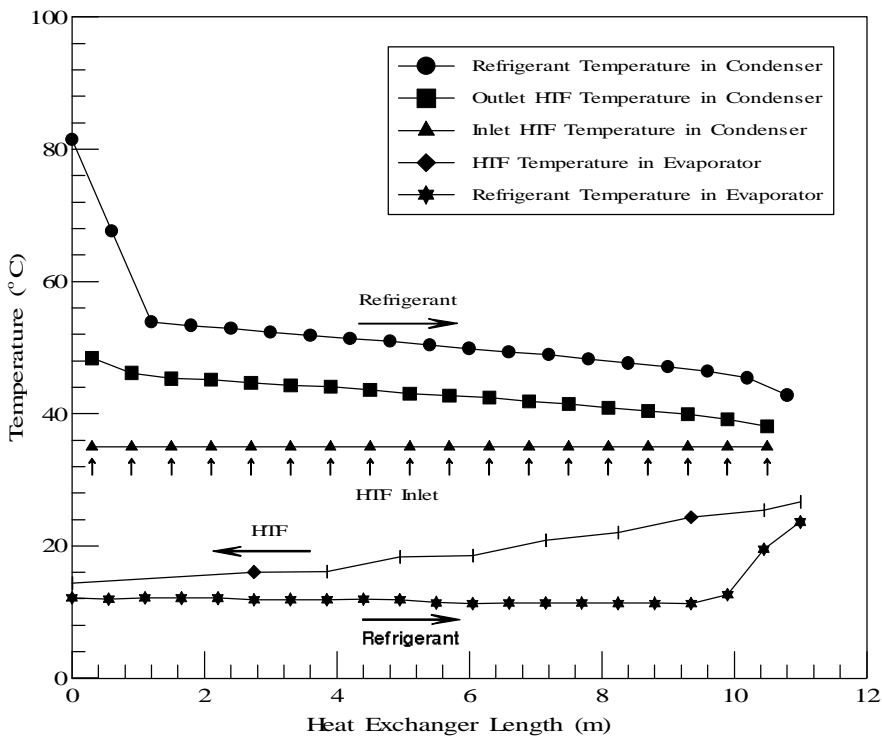


Figure 8. Temperature Distribution of R-407C in Cross-Flow Condenser and Counter-Flow Evaporator During the Cooling Test (Basic System, 1800 Compressor RPM)

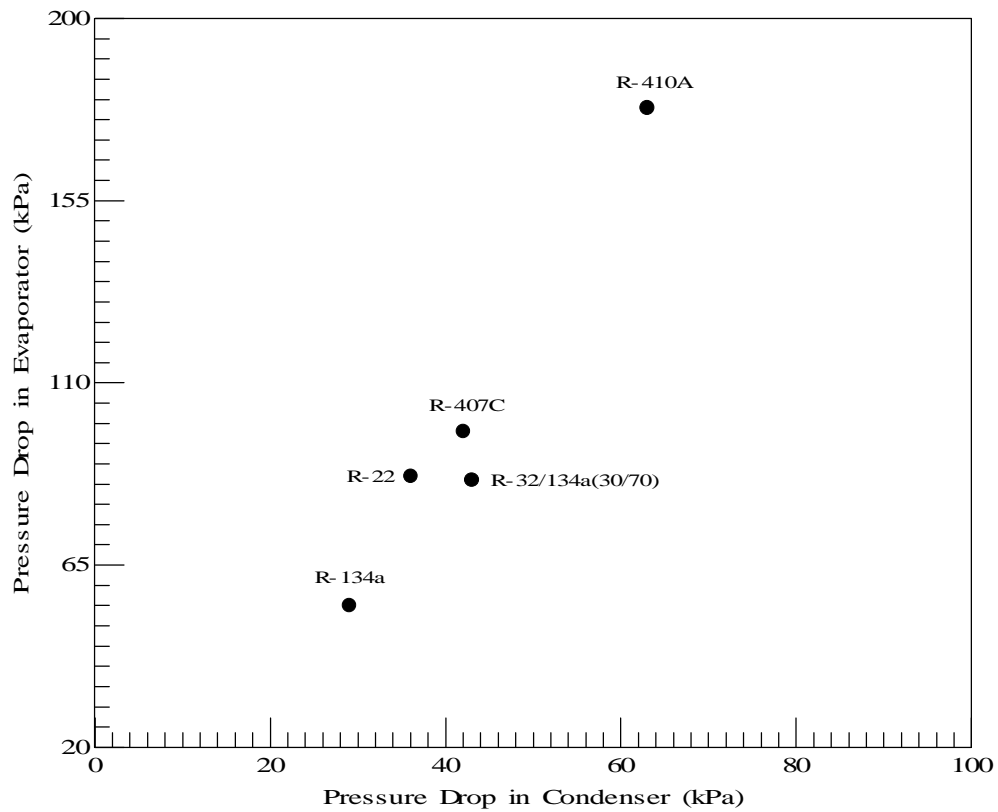


Figure 9. Refrigerant Pressure Drop in Cross-Flow Condenser and Counter-Flow Evaporator During the Cooling Test (Basic System, 1800 Compressor RPM)

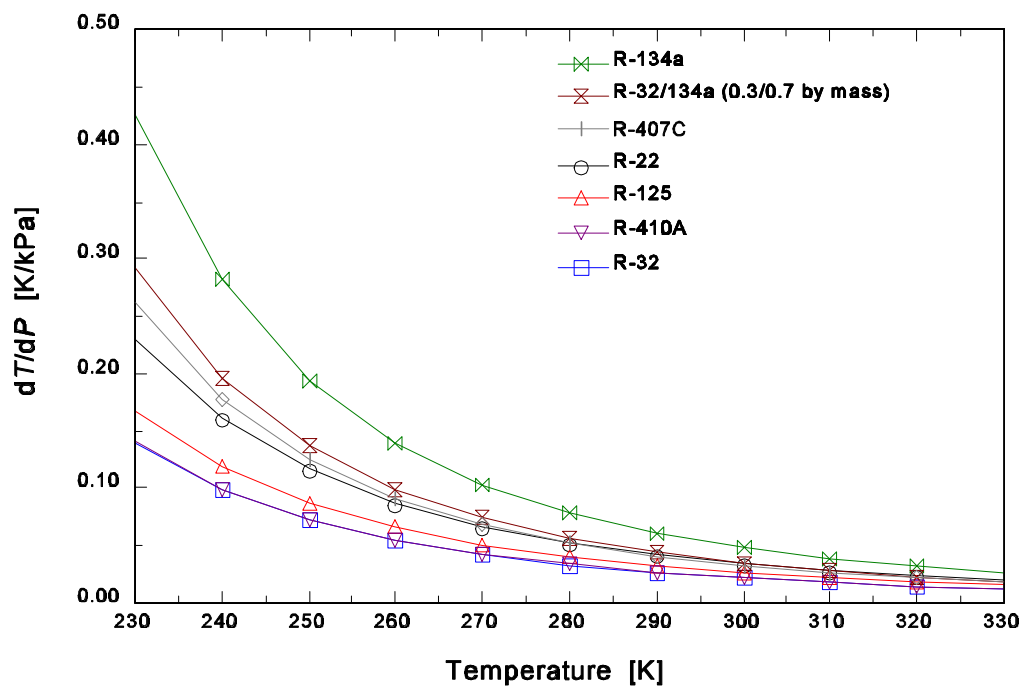


Figure 10. Dew Point dT/dP for Refrigerants Studied

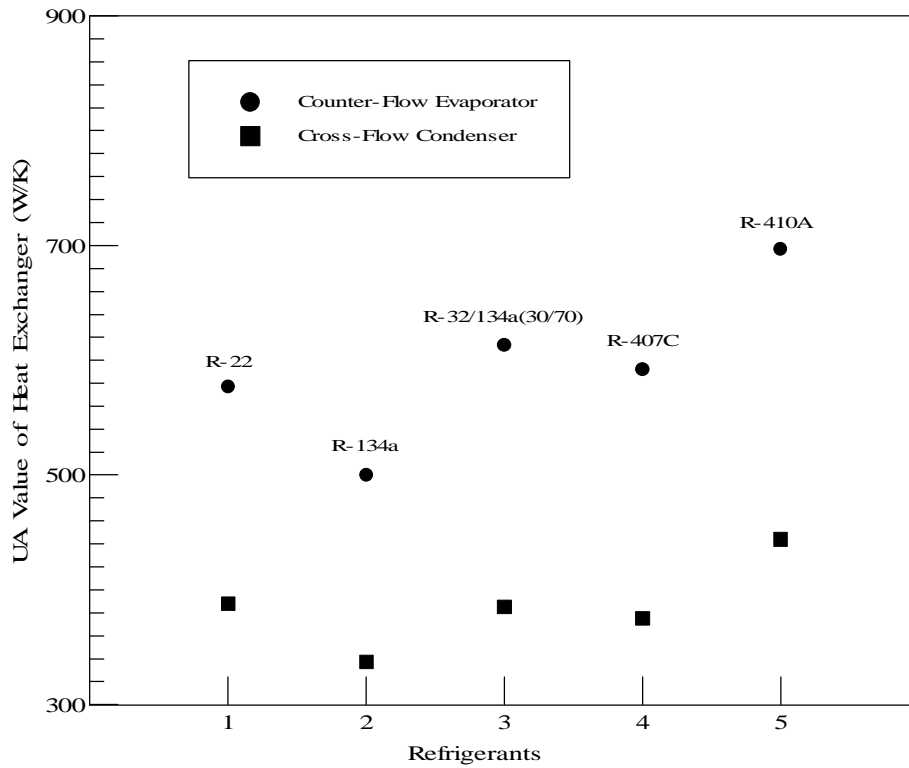


Figure 11. UA Values for Evaporator and Condenser During the Cooling Test (Basic System, 1800 Compressor RPM)

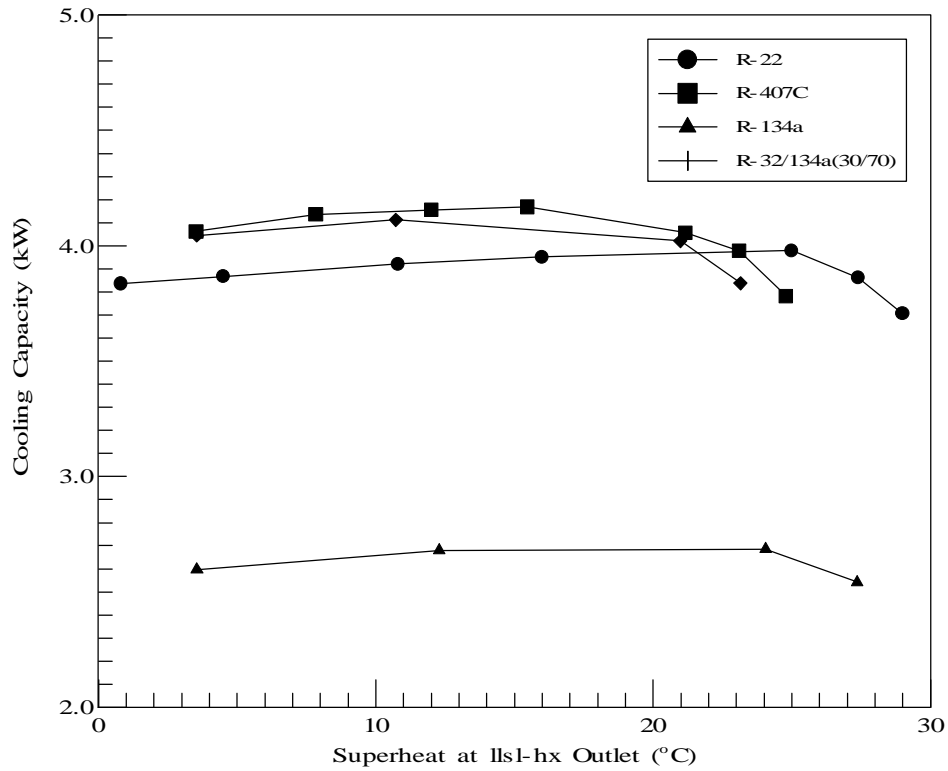


Figure 12. Capacity During the Cooling Test (System with LLSL-HX, 1800 Compressor RPM)

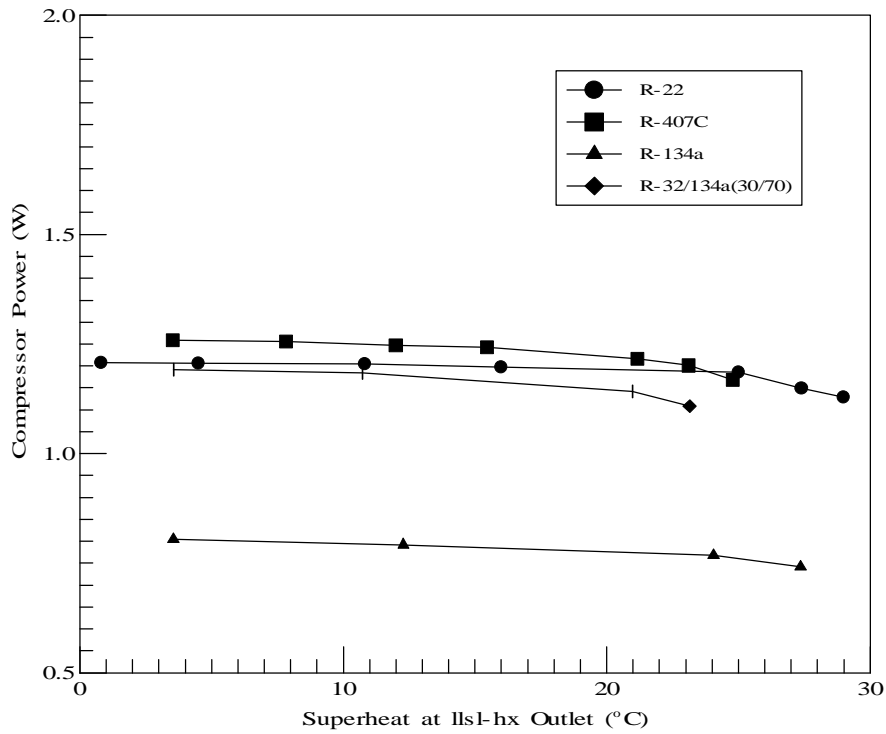


Figure 13. Compressor Power During the Cooling Test (System with LLSL-HX, 1800 Compressor RPM)

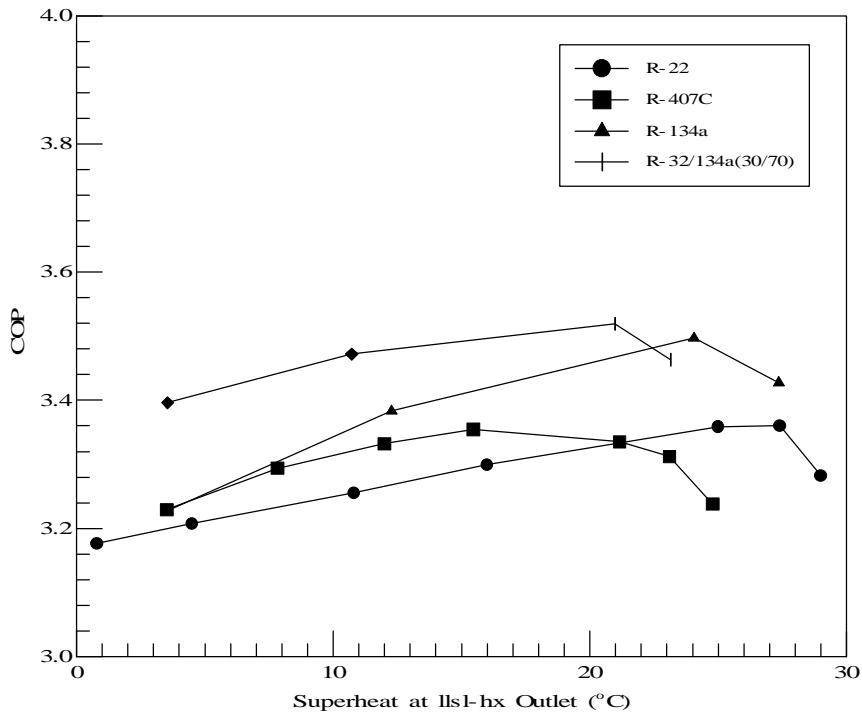


Figure 14. COP During the Cooling Test (System with LLSL-HX, 1800 Compressor RPM)

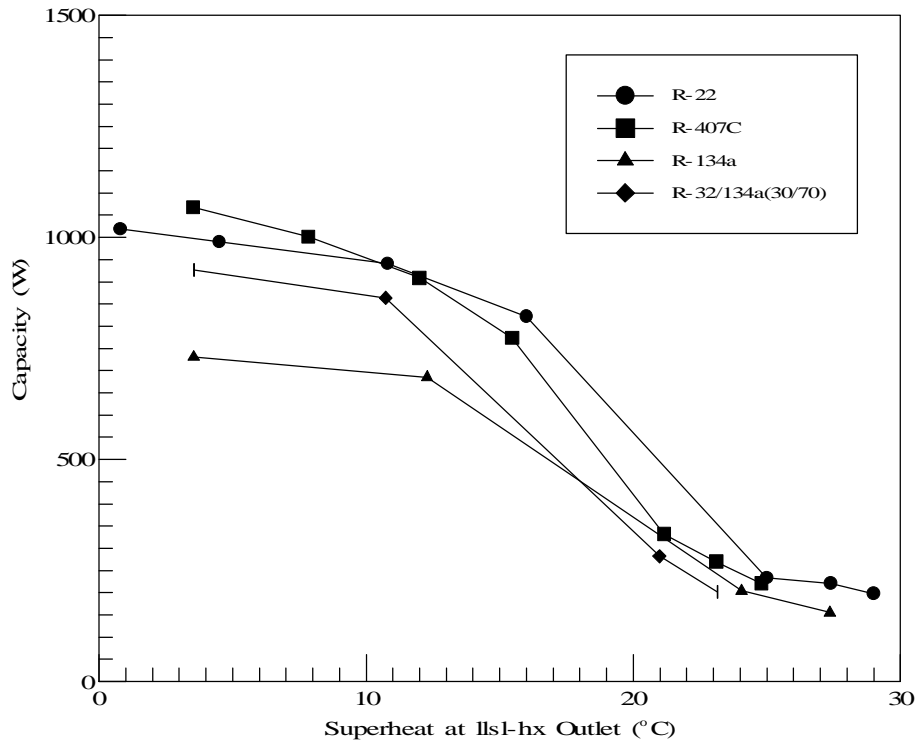


Figure 15. Capacity of LLSL-HX During the Cooling Test (1800 Compressor RPM)

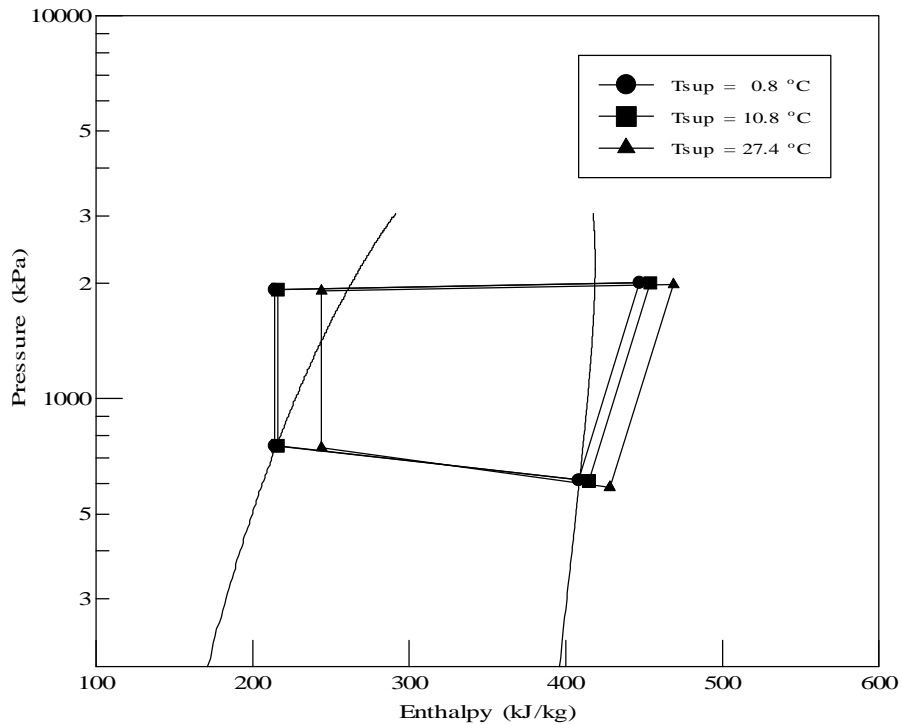


Figure 16. Pressure-Enthalpy Diagram for R-22 Diagram for R-22 During the Cooling Test at Different Superheats at the LLSL-HX Outlet (1800 Compressor RPM)

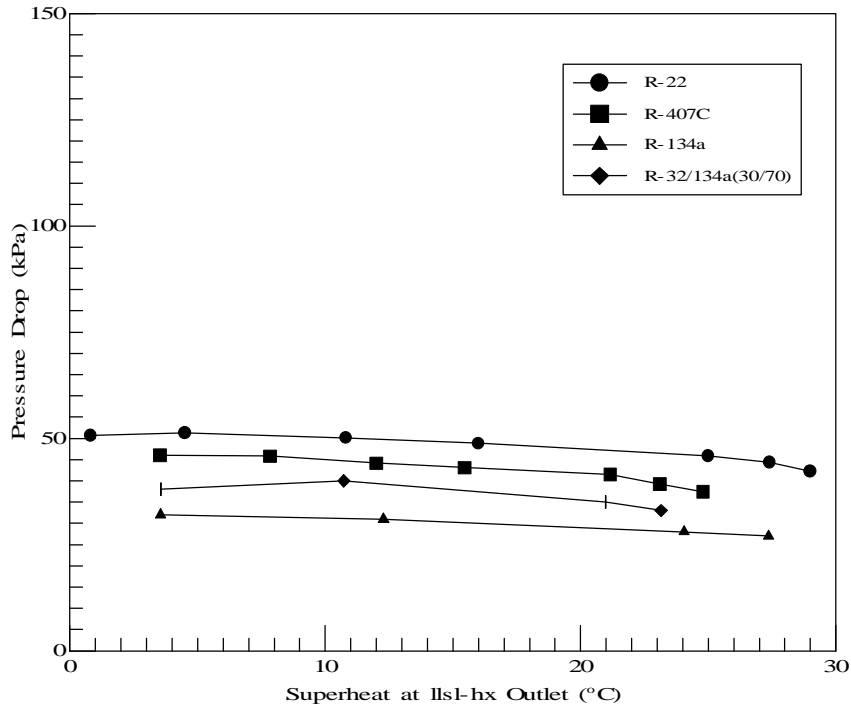


Figure 17. Refrigerant Pressure Drop in the Cross-Flow Condenser During the Cooling Test (System with LLSL-HX, 1800 Compressor RPM)

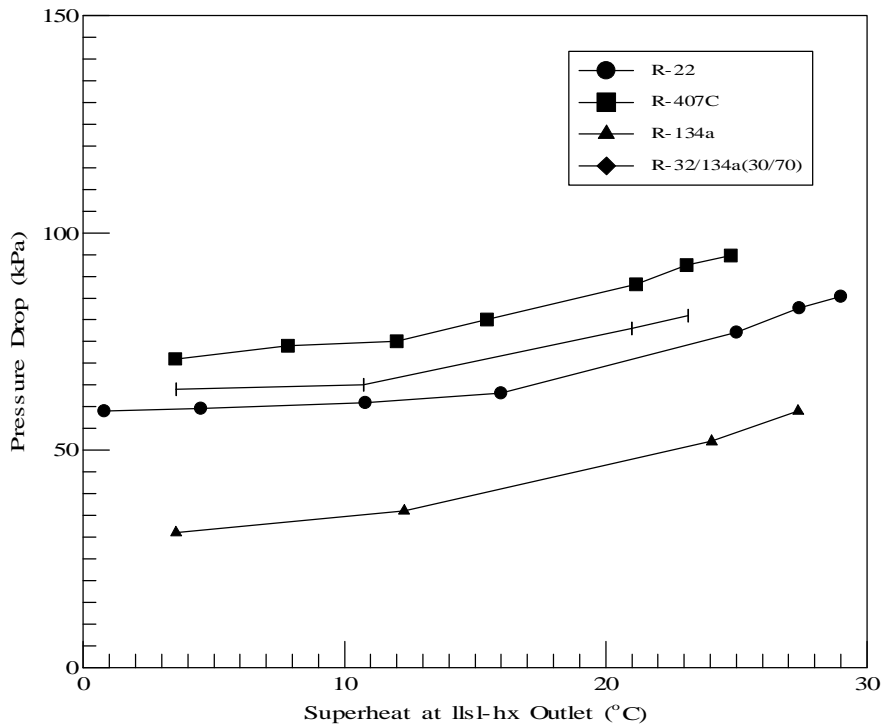


Figure 18. Refrigerant Pressure Drop in the Counter-Flow Evaporator During the Cooling Test (System with LLSL-HX, 1800 Compressor RPM)

8. APPENDIX. Data Uncertainty Information

The main test results characterizing the performance of refrigerants in the tested apparatus are capacity and COP, COP being the ratio of capacity to compressor power. To provide uncertainty information of the reported results, we performed an uncertainty analysis for R-22 cooling and heating tests at 1000 compressor speed (RPM). Table A1 contains the summary of this analysis. The cooling mode calculations contained in this appendix present the methodology used. All components of a standard uncertainty were evaluated by a Type B method [9].

Table A1. Summary of Uncertainty Analysis

(Relative expanded uncertainties calculated using standard uncertainties and a coverage factor $k=2$)

Parameter	Value and relative uncertainty	
Capacity	2570 W \pm 1.1%	(cooling)
	2213 W \pm 1.2%	(heating)
Compressor Power	603.3 W \pm 1.2%	(cooling)
	468.9 W \pm 1.5%	(heating)
Coefficient of Performance	4.26 \pm 1.6%	(cooling)
	4.72 \pm 1.9%	(heating)

8.1 Evaluation of Results Uncertainty for the Cooling Mode.

8.1.1 System capacity

During the cooling test, the system capacity was evaluated on the evaporator side using the following equation:

$$\dot{Q} = \dot{m} \cdot c_p \cdot \Delta T \quad (\text{A1})$$

where \dot{Q} is evaporator capacity (W), \dot{m} is a mass flow rate of the heat-transfer fluid (kg/s), c_p is specific heat of the heat-transfer fluid (J/(kg·°C)), and ΔT is the heat-transfer fluid temperature change through the evaporator (°C). Based on an RMS uncertainty propagation analysis:

$$u_c = \left[\left(\frac{\partial \dot{Q}}{\partial \dot{m}} u_{\dot{m}} \right)^2 + \left(\frac{\partial \dot{Q}}{\partial c_p} u_{c_p} \right)^2 + \left(\frac{\partial \dot{Q}}{\partial \Delta T} u_{\Delta T} \right)^2 \right]^{0.5} \quad (\text{A2})$$

Since $\partial \dot{Q} / \partial \dot{m} = c_p \Delta T$, $\partial \dot{Q} / \partial c_p = \dot{m} \Delta T$, and $\partial \dot{Q} / \partial \Delta T = \dot{m} c_p$ the equation for uncertainty of capacity assumes the following form:

$$u_{\dot{Q}} = [(c_p \Delta T u_{\dot{m}})^2 + (\dot{m} \Delta T u_{c_p})^2 + (\dot{m} c_p u_{\Delta T})^2]^{0.5} \quad (\text{A3})$$

Based on the manufacturer's literature and information obtained from a manufacturer's representative, the uncertainty of the mass flow meter is equal to $\pm 0.4\%$ of the flow rate (95% confidence level). For this example with $\dot{m} = 0.05918$ kg/s, the standard uncertainty $u_{\dot{m}} = 0.5 \cdot 0.004 \cdot 0.05918$ kg/s = 0.00012 kg/s.

Specific heat capacity for the heat-transfer fluid (60/40 water glycol solution) is calculated using a linear function fitted to manufacturer's data, $c_p (\text{J}/(\text{kg} \cdot ^\circ\text{C})) = 3460.68 + 3.4283T$, where T is the fluid's temperature in degrees Celsius. For this example, the average temperature of the HTF in the evaporator was $(26.7 \text{ }^\circ\text{C} + 14.4 \text{ }^\circ\text{C})/2 = 20.6 \text{ }^\circ\text{C}$, and the corresponding fluid's specific heat was 3531.3 J/(kg·°C). Pannock and Didion [2] estimated that the uncertainty of calculating specific heat (at a 99.7% confidence level) due to the uncertainty of the regression curve and temperature measurement is 9.4 J/(kg·°C). To account for the uncertainty of composition of the water/glycol solution, we adopted the value of 9.4 J/(kg·°C) as a standard uncertainty.

Gebbie [10] estimated the uncertainty of the ΔT measurement via a ten-function thermopile to be 0.04°C. We conservatively used the value of 0.05°C for the standard uncertainty. This value accounts for the uncertainty in temperature measurement by the reference thermocouple and data acquisition system. The temperature change, ΔT , in our example calculation was 12.3 °C.

Using the presented numbers in equation (A3) provides the following result for the combined standard uncertainty in capacity:

$$u_{\dot{Q}} = [(3531.3 \cdot 12.3 \cdot 0.00012)^2 + (0.05918 \cdot 12.3 \cdot 9.4)^2 + (0.05918 \cdot 3531.3 \cdot 0.05)^2]^{0.5} = 13.6 \text{ W}$$

Therefore, for approximately 95% confidence level we obtain:

$$\dot{Q} = 2570.0 \text{ W} \pm 27.2 \text{ W} \quad \text{or} \quad \dot{Q} = 2570.0 \text{ W} \pm 1.1 \%$$

where the numbers following the \pm sign are expanded uncertainties estimated by using the combined standard uncertainty of 13.6 W and the coverage factor of 2.

8.1.2. Compressor Power

Compressor power was obtained by measuring compressor speed and torque on the shaft and by applying the measured values to the following equation:

$$\dot{W}_{comp} = \frac{\pi}{30} \tau \cdot n \quad (\text{A4})$$

where \dot{W}_{comp} is compressor power (W), τ is compressor's shaft torque (N·m), and n is compressor speed (revolutions per minute). Based on an RMS uncertainty propagation analysis, the uncertainty of the compressor power, $u_{\dot{W}}$, can be calculated by the following equation:

$$u_{\dot{W}} = \left[\left(\frac{\pi}{30} \tau \cdot u_n \right)^2 + \left(\frac{\pi}{30} n \cdot u_\tau \right)^2 \right]^{0.5} \quad (\text{A5})$$

where u_n and u_τ are the uncertainties for measurement of the compressor speed and torque, respectively. Both measurements are provided by the torque meter.

According to the manufacturer's representative, the RPM counter is accurate to ± 1 count of the revolutions per minute indicated on the counter display (99.7% confidence level). Since this ± 1 count uncertainty does not include the analog input to the data acquisition system and no information was available about the distribution of calibration data, we conservatively used $u_n = \pm 3$ 1/minute for the standard uncertainty. Regarding torque measurement, the manufacturer's specifications indicate that the RMS uncertainty is 0.15% of the full scale, which results in the value of 0.06 N·m (99.7% confidence level). Since this value does not include the analog input to the data acquisition system and no information was available about the distribution of calibration data, we conservatively used the value of 0.03 N·m as the standard uncertainty.

During the cooling test with R-22, the compressor speed was 1000 revolutions per minute and the torque was 5.761 N·m. Using these numbers in equation (A5) yields the following for the combined standard uncertainty in compressor power:

$$u_{\dot{W}} = [(\pi \cdot 5.761 \cdot 3/30)^2 + (\pi \cdot 1000 \cdot 0.03/30)^2]^{0.5} = 3.6 \text{ W}$$

Therefore, for approximately 95% confidence level we obtain:

$$\dot{W}_{comp} = (\pi \cdot 5.761 \cdot 1000/30 \pm 7.2) \text{ W} = 603.3 \text{ W} \pm 7.2 \text{ W} \quad \text{or} \quad \dot{W}_{comp} = 603.3 \text{ W} \pm 1.2\%$$

where the numbers following the \pm sign are expanded uncertainties estimated by using the combined standard uncertainty of 3.6 W and the coverage factor of 2.

8.1.3 Coefficient of Performance

The cooling COP is calculated by the following equation:

$$\text{COP} = \frac{\dot{Q}}{\dot{W}_{comp}} \quad (\text{A6})$$

After having performed the appropriate partial derivatives, an uncertainty propagation analysis of equation (A6) yields:

$$u_{\text{COP}} = \left[\left(\frac{u_{\dot{Q}}}{\dot{W}_{comp}} \right)^2 + \left(\frac{-\dot{Q}}{\dot{W}_{comp}^2} u_{\dot{W}} \right)^2 \right]^{0.5} \quad (\text{A7})$$

For the numbers presented in this appendix, equation (A7) yields the following for the combined standard uncertainty in the COP:

$$u_{\text{COP}} = [(13.6/603.3)^2 + (2570 \cdot 3.6/603.3^2)^2] = 0.034$$

Therefore, for approximately 95% confidence level we obtain:

$$\text{COP} = 2570/603.3 \pm 2 \cdot 0.034 = 4.26 \pm 0.07 \quad \text{or} \quad \text{COP} = 4.26 \pm 1.6\%$$

where the numbers following the \pm sign are expanded uncertainties estimated by using the combined standard uncertainty of 0.034 and the coverage factor of 2.